PAPER

Check for updates

Insight into the interdependence of Ni and Al in bifunctional Ni/ZSM-5 catalysts at the nanoscale†

Hue-Tong Vu, ‡[a] Iztok Arčon,‡[bc] Danilo Oliveira de Souza, [d] Simone Pollastri, [d] Goran Dražić, [a] Janez Volavšek,[a] Gregor Mali, [a] Nataša Zabukovec Logar [ab] and Nataša Novak Tušar [*ab]

Catalyst design is crucial for improving catalytic activity and product selectivity. In a bifunctional Ni/ZSM-5 zeolite type catalyst, catalytic properties are usually tuned *via* varying Al and Ni contents. While changes in acid properties associated with Al sites are usually closely investigated, Ni phases, however, receive inadequate attention. Herein, we present a systematic structural study of Ni in the Ni/ZSM-5 materials by using Ni K-edge XANES and EXAFS analyses, complemented by XRD and TEM, to resolve the changes in the local environment of Ni species induced by the different Al contents of the parent ZSM-5 prepared by a "green", template free technique. Ni species in Ni/ZSM-5 exist as NiO crystals (3–50 nm) and as charge compensating Ni^{2+} cations. The Ni K-edge XANES and EXAFS results enabled the quantification of Ni-containing species. At a low Al to Si ratio ($n_{Al}/n_{Si} \leq 0.04$), the NiO nanoparticles predominate in the samples and account for over 65% of Ni phases. However, NiO is outnumbered by Ni^{2+} cations attached to the zeolite framework in ZSM-5 with a high Al to Si ratio ($n_{Al}/n_{Si} = 0.05$) due to a higher number of framework negative charges imparted by Al. The obtained results show that the number of highly reducible and active NiO crystals is strongly correlated with the framework Al sites present in ZSM-5 zeolites, which depend greatly on the synthesis conditions. Therefore, this kind of study is beneficial for any further investigation of the catalytic activities of Ni/ZSM-5 and other metal-modified bifunctional catalysts.

Introduction

In light of the 2030 Agenda for Sustainable Development first introduced by the United Nations Member States in 2015, green chemistry has been pushed forward as part of a multidisciplinary effort to achieve the 17 goals.[1] Green chemistry can be considered as a guideline to achieve sustainability in process developments and chemical production.[2] Accordingly, the use of environmentally hazardous chemicals and generation of waste should be avoided. In pursuance of a zero-waste process, it is important to increase product efficiency and thus prevent wastage of resources. In this view, catalyst design has become indispensable in chemical production in order to increase the yield of desired products as well as reduce side products.[4,5]

Zeolites are important catalysts in the chemical industry owing to their different beneficial properties.[6,7] The greatly porous structure of zeolites which is composed of long-range interconnected SiO_4 and AlO_4 tetrahedra offers a high specific surface area leading to high dispersion of supported active metals.[8] The presence of Al in zeolitic lattices induces framework negative charges, which can then be neutralized by different charge compensating cations, *i.e.*, H^+ (forming Brønsted acid sites) and extra framework cations (Lewis acid sites). The acid properties of zeolites can be regulated by simply varying the molar ratio of Al to Si in the zeolite frameworks in order to drive the catalytic reactions towards desired products.[9] Moreover, the isomorphous substitution of Si with Al in the tetrahedral units provides acidity as well as ion exchange ability, which can prevent supported metals from leaching due to strong interaction with zeolitic supports.[10] The combination of zeolites and active metals results in bifunctional catalytic systems, which have been reported in many studies for their excellent activity.[11] Among these, ZSM-5 zeolites functionalized with transition metal Ni (Ni/ZSM-5), a cheap and abundant metal, stand out as highly active and cost-effective catalysts.[12–17] Furthermore, the great (hydro)thermal stability under harsh working conditions, *e.g.*, temperature up to 873 K and pressure ≤60 bar (Table 1), makes this Si-rich zeolitic bifunctional

[a] National Institute of Chemistry, Hajdrihova 19, 1000 Ljubljana, Slovenia. E-mail: natasa.novak.tusar@ki.si

[b] University of Nova Gorica, Vipavska 13, 5000 Nova Gorica, Slovenia

[c] Jožef Stefan Institute, Jamova cesta 39, 1000 Ljubljana, Slovenia

[d] Elettra - Sincrotrone Trieste, s. s. 14, km 163.5 Basovizza, Trieste, 34149, Italy

† Electronic supplementary information (ESI) available. See https://doi.org/10.1039/d2na00102k

‡ These authors contributed equally to this work and are both considered first authors.

Table 1 Examples of literature focused on Ni/ZSM-5 and its utilization in different catalytic applications published between 1997 and 2021

No	n_{Al}/n_{Si}	XPS/XAS	ωNi/wt%	Catalytic application	T/K	p/bar	Ref
1	0.08	Yes	0.4–6	Cracking of n-/iso-butane	773	1	18–20
2	0.05	No	1–5	Toluene hydrogenation	643–673	60	21 and 22
3	0.07	No	1–6	Catalytic pyrolysis of biomass	773	1	23
4	0.07	Yes	2	Ethane aromatization	823	1	24
5	0.04	Yes	1–4	Hydroconversion of n-heptane	560	1	25
6	0.04	No	0.6	Aromatization of n-pentane	773	1	26
7	0.07	No	9	Hydrogenation of oleic acid	633	40	27
8	0.07	No	5	Conversion of (methyl)-naphthalene	643	1	28
9	0.02	No	5	Catalytic decomposition of ammonia	873	1	29
10	0.025	No	10	Conversion of γ-valerolactone	523	1	30
11	0.025	No	1–2	n-octane hydroconversion	548–578	40	31
12	0.06	No	1.4	Catalytic conversion of n-hexane	498–648	1	32
13	0–0.07	No	5	CO_2 methanation	523–673	1	33
14	0.01–0.03	No	1.9–4.2	Hydrodeoxygenation of palmitic acid	533	40	34
15	0.03–0.05	No	5	Hydrodeoxygenation of guaiacol	513	40	35
16	0.015–0.08	No	2	Co-aromatization of n-pentane and methanol	748	1	36

catalyst more attractive, especially, for vapor phase applications that are relevant for industries.

It is inevitable that bifunctional Ni/ZSM-5 catalysts have been intensively investigated as exemplarily shown in Table 1. In most of the studies, the relation between Al content and the catalytic activity of the Ni/ZSM-5 catalysts was investigated closely, while neglecting changes in Ni phases in association with Al content. The chemical nature of Ni phases, which is also essential for the understanding of the catalyst's behaviour, is usually evaluated indirectly by its temperature-dependent reducibility using temperature-programmed reduction with H_2 (H_2-TPR). Typically, a H_2-TPR profile displays two peaks, one at low temperature (<633 K) corresponding to highly reducible NiO and the other at high temperatures (>723 K), which is ambiguously ascribed to Ni^{2+} cations interacting with the zeolite framework.[28,35] There are only a few studies that included thorough analyses using X-ray absorption spectroscopy (XAS) and/or X-ray photoelectron spectroscopy (XPS) to elucidate the local environment and the chemical state of Ni species. The reported results are, however, limited to the identification of the two Ni-containing phases as suggested by H_2-TPR results.[18–20,24,25,27] The quantitative evaluation of the influence of Al content on the Ni phases in Ni/ZSM-5 has not been conducted and published from 1997 until now. On the other hand, the variation of Al content also leads to alteration in Al distribution,[37] morphology[38] and possibly Ni phases. The location, nature and the local environment of Al in zeolites were reported to greatly depend on the hydrothermal synthesis conditions.[37] Therefore, more investigations using advanced characterization techniques, e.g., nuclear magnetic resonance (NMR), XAS and/ or XPS, are required to reveal the interdependence of Ni and Al sites in the Ni/ZSM-5 bifunctional catalysts.

In this study, we focused on the interplay between the Al content and Ni phases of Ni/ZSM-5 catalysts. A series of ZSM-5 type zeolites with different Al to Si molar ratios (n_{Al}/n_{Si} = 0.03, 0.04 and 0.05) were synthesized by a "green" method, i.e., a seed-assisted hydrothermal technique without an unfavorable organic template. Subsequently, the obtained ZSM-5 zeolites were loaded with different amounts of Ni (resulting in Ni to Si molar ratios of 0.01, 0.03 and 0.05) via incipient wetness impregnation. A systematic study using Ni K-edge XANES (X-ray absorption near edge structure) and EXAFS (extended X-ray absorption fine structure) was carried out to monitor the local structure and chemical state of Ni species in the catalysts. Furthermore, transmission electron microscopy (TEM) was employed to examine the morphology of the catalysts. Such combined structural analysis provided an in-depth understanding of the influence of Al and Ni contents on the formation of different Ni phases in Ni/ZSM-5 at the molecular scale.

Results and discussion

Structural properties

In order to investigate the relation of Ni and ZSM-5 zeolites, a series of ZSM-5 zeolites with different molar ratios of Al to Si (n_{Al}/n_{Si} = 0.03 or 0.04 or 0.05) were synthesized using a template-free hydrothermal method.[39] The obtained materials, i.e., 03ZSM-5, 04ZSM-5 and 05ZSM-5, with the corresponding elemental composition determined by SEM-EDX are listed in Table 2. By gradually increasing the amount of the Al precursor (aqueous solution of sodium aluminate) in the synthesis gels, three solids were obtained, which exhibited considerably different Al contents, i.e., 1.4, 1.8 and 2.7 wt%, leading to ascending n_{Al}/n_{Si} from 0.03 to 0.08. The structure of the three solids was examined by XRD. The recorded XRD patterns display sharp and distinct diffraction reflections suggesting a highly crystalline structure (Fig. 1). The reflexes at 2θ of 7.9°, 8.9°, 23.0° and 23.8°, which can be indexed to the planes (011), (200), (501) and (303), respectively, characteristic of ZSM-5, are observed for all samples. No other phase was detected. Thus, it is concluded that irrespective of n_{Al}/n_{Si}, the highly crystalline ZSM-5 phase predominates in all samples. Further investigation using ^{27}Al-NMR reveals that the majority of Al species in the ZSM-5 zeolites are present as tetrahedral Al

Table 2 Al to Si ratio (n_{Al}/n_{Si}), elemental content (wNi and wAl in wt%) and the fraction of Al species (tetrahedral Al (Al$^{[IV]}$) and octahedral Al (Al$^{[VII]}$)) of ZSM-5 zeolites

Catalysts	n_{Al}/n_{Si}[a]	wAl[a]/wt%	wNi[a]/wt%	Fraction[b]/% Al$^{[IV]}$	Al$^{[VI]}$
03ZSM-5	0.03	1.4	0	95	5
Ni/03ZSM-5-1	0.03	1.4	0.4	—	—
Ni/03ZSM-5-3	0.03	1.2	1.3	—	—
Ni/03ZSM-5-5	0.03	1.3	3.7	—	—
04ZSM-5	0.05	1.8	0	95	5
Ni/04ZSM-5-1	0.05	1.7	0.8	—	—
Ni/04ZSM-5-3	0.05	1.7	1.6	—	—
Ni/04ZSM-5-5	0.05	1.8	3.4	—	—
05ZSM-5	0.08	2.7	0	84	16
Ni/05ZSM-5-1	0.08	2.7	0.6	—	—
Ni/05ZSM-5-3	0.08	2.3	1.7	—	—
Ni/05ZSM-5-5	0.08	2.5	3.5	—	—

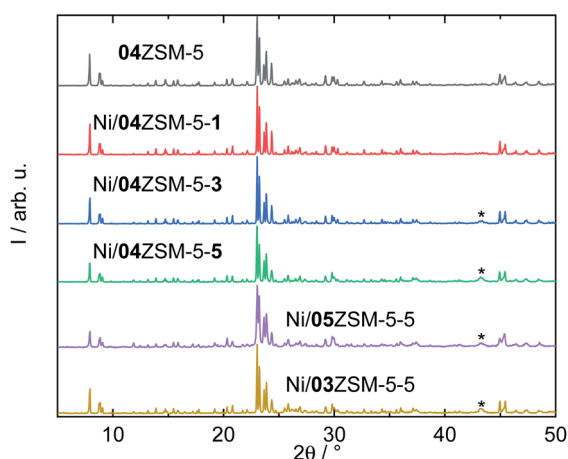[a] Determined by SEM-EDX. [b] Determined by ^{27}Al-NMR.

Fig. 1 XRD patterns of selected ZSM-5 zeolites with the asterisks mark the diffraction reflection of NiO (PDF#01-089-5881).

(Al$^{[IV]}$), in addition to a small fraction of octahedral Al (Al$^{[VI]}$) as shown in Fig. S1.† With increasing the n_{Al}/n_{Si} ratio of the synthesis mixtures, the fraction of octahedral Al associated with the extra framework Al (EFAl) increases (Table 2). This is probably due to the disrupted crystallization rate at the high concentration of Al in the synthesis gel, which is known for MFI-type zeolites.[40] Despite the increasing contribution of EFAl, the specific amount of tetrahedrally coordinated Al species is proportional to the n_{Al}/n_{Si} ratio, which is 1.33, 1.71 and 2.27 wt% for 03ZSM-5, 04ZSM-5 and 05ZSM-5, respectively.

Subsequently, Ni was introduced into all three samples by incipient wetness impregnation, aiming at three different molar ratios of Ni to Si. Taking 04ZSM-5 as an example, after impregnation, a series of ZSM-5 samples functionalized with ascending Ni content, i.e., Ni/04ZSM-5-1, Ni/04ZSM-5-3 and Ni/04ZSM-5-5 with Ni contents of 0.8, 1.6 and 3.4 wt%, respectively, are obtained. Similarly, two other series were also prepared for 03ZSM-5 and 05ZSM-5 (Table 2). Despite the different Ni

contents, the structure of ZSM-5 remains highly crystalline for all the samples as suggested by the XRD patterns, e.g., for the series of 04ZSM-5 (Fig. 1). It is noted that at low Ni content (≤0.8 wt%), e.g., in Ni/04ZSM-5-1, the NiO phase cannot be detected by XRD. However, at higher Ni content, a broad diffraction reflex at 2θ of 43.3° corresponding to the (200) plane of NiO (PDF#01-089-5881) is observed probably due to an increase in the NiO content and crystal size. This indicates that Ni introduced in ZSM-5 zeolites exists in the form of nano NiO crystals, where the NiO crystal sizes grow with increasing Ni content. However, it is not excluded that other Ni phases without a long range order are present, e.g., amorphous Ni-containing complexes, extra framework Ni cations or metallic Ni nanoparticles.

Textural properties

The textural properties, which are important factors influencing catalyst's activity, were also investigated for the ZSM-5 supports. A type-I isotherm coupled with an H4 hysteresis loop was recorded, suggesting a bimodal pore structure, i.e., micro and mesopores (Fig. 2). Therefore, the non-local density functional theory (NLDFT) was employed to determine the pore structure.[41] It is revealed that micropores dominate in all the tested samples as shown in Table 3. Regardless of Al to Si ratios, a similar specific total pore volume (0.20–0.22 cm^3 g^{-1}) and a pore structure comprising 70% of micropores and 30% of mesopores are observed in the N$_2$ sorption results. Further evaluation using the Brunauer–Emmett–Teller (BET) model also shows analogous specific surface areas (408–451 m^2 g^{-1}) for 03ZSM-5, 04ZSM-5 and 05ZSM-5. These findings indicate that the variation of Al to Si ratios in the range from 0.03 to 0.05 has a marginal effect on the textural properties of the obtained ZSM-5.

Regarding the influence of the Ni introduction on the textural properties of the parent ZSM-5 material, the Ni/04ZSM-5-5 sample possessing the highest Ni content of the Ni/04ZSM-5 series was exemplarily examined. In comparison with 04ZSM-5, Ni/04ZSM-5-5 exhibits an almost identical N$_2$ sorption isotherm, resulting in comparable textural properties, i.e., A_{BET}
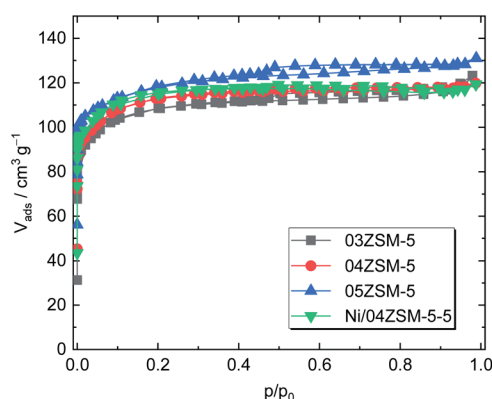

Fig. 2 N$_2$ sorption isotherms of ZSM-5 zeolites (03ZSM-5, 04ZSM-5 and 05ZSM-5) and ZSM-5 with Ni (Ni/04ZSM-5-5).

Table 3 Specific surface area (A_{BET}) and the specific total/micro/meso pore volume ($V_{p/micro/meso}$) of ZSM-5 zeolites

Samples	$A_{BET}/m^2 \, g^{-1}$	$V_p/cm^3 \, g^{-1}$	$V_{micro}/cm^3 \, g^{-1}$	$^a V_{meso}/cm^3 \, g^{-1}$
03ZSM-5	408	0.20	0.14	0.06
04ZSM-5	410	0.20	0.15	0.05
05ZSM-5	451	0.22	0.17	0.05
Ni/04ZSM-5-5	425	0.20	0.16	0.04

^{a} $V_{meso} = V_p - V_{micro}$.

$= 425 \, m^2 \, g^{-1}$ and $V_p = 0.20 \, cm^3 \, g^{-1}$. This suggests that the impregnation of Ni (Ni content ≤3.4 wt%) does not affect the textural properties of ZSM-5 zeolites.

Nature of Ni impregnated on ZSM-5

TEM and elemental analyses

The morphology of Ni/04ZSM-5-3 and Ni/05ZSM-5-1 was selectively analyzed by STEM and EDXS. As mentioned above, the NiO phase is hardly visible in the XRD patterns of these catalysts (Fig. 1). However, the HAADF-STEM images (Fig. 3c) clearly show that the NiO nanoparticles are present with a size between 3 and 50 nm and uniformly distributed over the ZSM-5 support. Some particles are aggregated as shown in Fig. 3b and c, indicating a partial sintering/coalescence of the nanoparticles during sample preparation.

To confirm that the observed nanoparticles are indeed NiO, we performed EDXS elemental mapping (Fig. 3d), where the K_α signal for Ni matches very well with that of the nanoparticles, which are shown as a bright area in Fig. 3c. The signal for oxygen is not as specific because the support also contains large amounts of oxygen. No other Ni rich phase was detected. On the other hand, the sample Ni/05ZSM-5-1 contains no NiO nanoparticles of 3–50 nm and has uniformly distributed Ni as shown in Fig. 3i–p.

Ni K-edge XANES analysis

Ni K-edge XANES is used to monitor the valence state and local symmetry of Ni cations in the Ni functionalized zeolite Ni/ZSM-5 samples. Fig. 4 displays the normalized Ni K-edge XANES spectra, in addition to the spectra of corresponding Ni reference compounds (crystalline NiO, NiO nanoparticles and metallic Ni).

Different local environments of Ni cations result in different K-edge profiles in the XANES spectra, and the energy position of the Ni K-edge is correlated with the valence state of the Ni cations in the sample. The energy of the Ni K-edge is shifted to higher energies by approximately 2 eV per valence state.[42] The Ni K-edge edge profile and energy position of all Ni/ZSM-5 samples indicate that the Ni species are in the divalent form octahedrally coordinated with oxygen atoms, as in the NiO crystalline reference sample.

The Ni K-edge profiles of Ni/ZSM-5 samples are very similar, but not identical. Principal component analysis (PCA) of the XANES spectra of the catalysts indicates that a linear
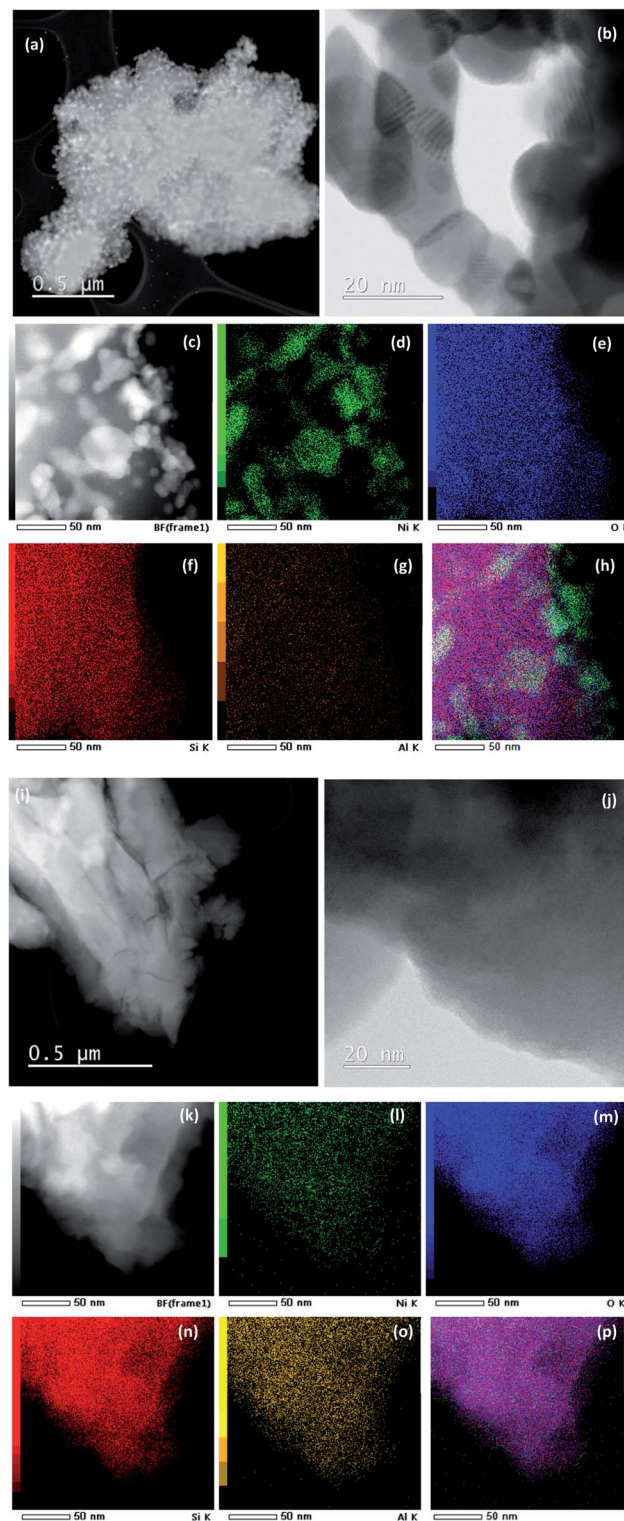

Fig. 3 (a) High-angle annular dark-field scanning transmission electron microscopy (HAADF-STEM) micrograph; (b) bright field (BF)-STEM micrograph; (c) HAADF-STEM micrograph, the corresponding EDX elemental mapping (for Ni (d), O (e), Si (f) and Al (g)) and the overlaid image (h) of Ni/04ZSM-5-3. (i) HAADF-STEM micrograph; (j) BF-STEM micrograph; (k) HAADF-STEM micrograph, the corresponding EDX elemental mapping (for Ni (l), O (m), Si (n) and Al (o)) and the overlaid image (p) of Ni/05ZSM-5-1.
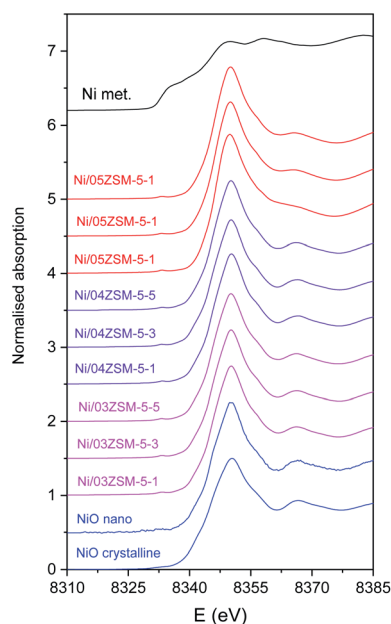
Fig. 4 Normalized Ni K-edge XANES spectra of Ni functionalized zeolite Ni/ZSM-5 samples. The spectra of reference crystalline NiO , NiO nanoparticles on the CeO₂ support and metallic Ni are shown for comparison.

Table 4 Relative amount of the two reference XANES profiles (NiO nanoparticles and Ni/05ZSM-5-1) obtained by LCF. Uncertainty of relative amounts is ±1%

Samples	LCF reference spectra	
	NiO nanoparticles	Ni/05ZSM-5-1
Ni/03ZSM-5-1	72%	28%
Ni/03ZSM-5-3	72%	28%
Ni/03ZSM-5-5	72%	28%
Ni/04ZSM-5-1	68%	32%
Ni/04ZSM-5-3	81%	19%
Ni/04ZSM-5-5	66%	34%
Ni/05ZSM-5-1	0%	100%
Ni/05ZSM-5-3	28%	72%
Ni/05ZSM-5-5	39%	61%

The XANES results thus demonstrate that all catalyst samples contain two Ni^{2+} species in different relative ratios. To identify the structure of the two Ni^{2+} species, Ni K-edge EXAFS analysis was used and complemented with the results of XRD and STEM/EDX.

Ni K-edge EXAFS analysis

Ni K-edge EXAFS analysis is used to directly monitor the average local environment of Ni cations in the Ni functionalized zeolite Ni/ZSM-5 samples. The k^3-weighted EXAFS spectra are plotted in the k space In Fig. S2, ESI.† In the Fourier transform (FT) magnitude of the EXAFS spectra (Fig. 6), the contributions of photoelectron scattering on the nearest shells of neighbours around the Ni atoms are observed in the R range up to about 5 Å. Already by a qualitative comparison of the FT EXAFS spectra, the differences in average Ni neighbourhoods between the samples can be observed. All samples, except Ni/05ZSM-5-1, exhibit a local Ni neighbourhood characteristic of crystalline NiO with a FCC crystal structure,[43] as in the crystalline NiO reference. However, the intensity of the second and more distant Ni coordination shells' contributions is smaller than those in the bulk NiO crystals, indicating that the average coordination numbers of the second and more distant coordination shells around Ni cations are significantly lower than that in the bulk NiO. The spectrum of the Ni/05ZSM-5-1 sample exhibits a significantly different local structure. The strong signal of the nearest coordination shell and a relatively weak signal from more distant coordination shells are detected (Fig. 6 and S3†).

Structural parameters of the average local Ni neighbourhood (the type and average number of neighbours; the radii and Debye–Waller factor of neighbour shells) are quantitatively resolved from the EXAFS spectra by comparing the measured EXAFS signal with the model signal, constructed *ab initio* with the FEFF6 program code.[44] A combined FEFF model is used, composed of neighbour atoms at distances characteristic of the expected Ni^{2+} species: crystalline NiO nanoparticles and Ni^{2+} cations attached to the zeolite framework *via* Ni–O–Si bridges. The atomic species of neighbours are identified in the fit by their specific scattering factor and phase shift.

combination of two different components is sufficient to completely describe each XANES spectrum in the series. The linear combination fit (LCF) analysis shows that a linear combination of the XANES profiles of the NiO nanoparticles on the CeO₂ support and Ni/05ZSM-5-1 sample can completely describe the XANES spectra of all the samples. The goodness of the LCF fit is illustrated in Fig. 5 for the XANES spectrum of the Ni/05ZSM-5-5 sample. The complete results of LCF analysis are listed in Table 4.
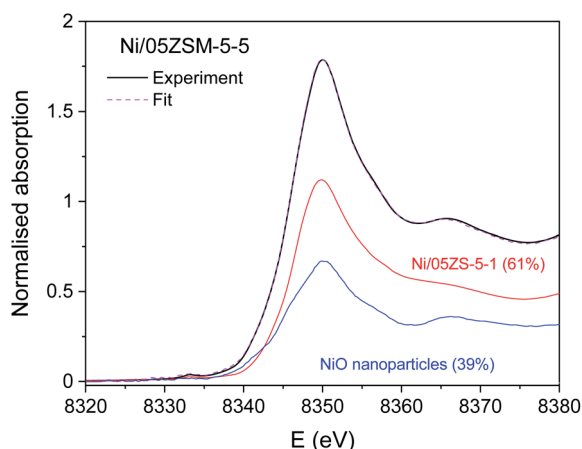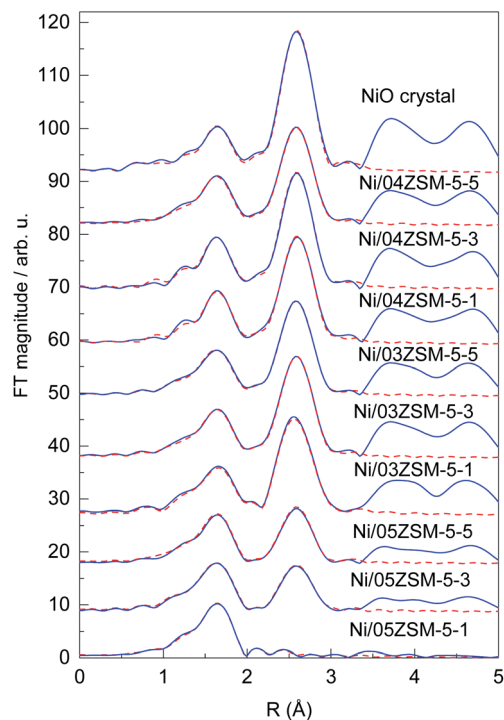

Fig. 5 Ni K-edge XANES spectrum of Ni/05ZSM-5-5: black solid curve: experiment; pink dashed line: best fit with linear combination of the reference XANES profiles; red solid curve: NiO nanoparticles on the CeO₂ support as a reference for Ni^{2+} in NiO crystalline nano-particles (39%); blue solid curve: Ni/05ZSM-5-1 as a reference for Ni^{2+} attached to the zeolite framework (61%).

Fig. 6 Fourier transform magnitude of the k^3-weighted Ni K-edge EXAFS spectra of the Ni functionalized ZSM-5 zeolite samples, calculated in the k range of 3–14 Å^{-1}. The spectrum of the reference crystalline NiO is added for comparison. Experiment – (blue solid line); the best fit EXAFS model calculated in the R range of 1.2 to 3.3 Å – (red dashed line).

The FEFF model for the crystalline NiO nanoparticles is based on the cubic crystal structure of NiO with the space group $Fm3m$ with the lattice constant $a = 4.177$ Å,[43] where Ni is coordinated with 6 oxygen atoms at a distance of 2.09 Å, 12 Ni atoms at 2.95 Å and 8 oxygen atoms at 3.62 Å. The FEFF model comprised three single scattering and two significant multiple scattering paths up to 3.6 Å, with 8 variable parameters: coordination shell distance (R) and Debye–Waller factors (σ^2) of all single scattering paths, and the amplitude reduction factor S_0^2 and shift of the energy origin of the photoelectron ΔE_o, common to all scattering paths, are introduced.

The model is tested on the EXAFS spectrum measured for the crystalline NiO. The shell coordination numbers were fixed to the crystallographic values in the fit, and the structural parameters of multiple scattering paths are constrained to those of the corresponding single scattering paths. A very good EXAFS fit (Fig. 6) is obtained in the k range of 3–14 Å^{-1} and the R-range of 1.2–3.3 Å. The best fit structural parameters are given in Table S1.†

The same FEFF model is used to fit the EXAFS spectrum of the reference sample with NiO nanoparticles on the CeO$_2$ support. The model contained all scattering paths used in the fit of the crystalline NiO, in which the coordination numbers of each shell were also allowed to vary. A very good EXAFS fit (Fig. S2†) is obtained in the k range of 3–11 Å^{-1} and the R-range of 1.2–3.3 Å. The best fit structural parameters, listed in Table

S2,† show that the reference sample contains crystalline NiO nanoparticles with cubic crystal structures with average particle sizes larger than 2 nm, as estimated from the average coordination number of Ni neighbours in the second coordination shell, using the relationships for cubic NiO nanoparticles reported by Kuzmin and Chaboy.[45]

For the spectrum of the Ni/05ZSM-5-1 sample, which shows a significantly different Ni local structure, a separate FEFF model was constructed, with octahedral coordination of 6 oxygen atoms in the nearest Ni coordination shell at a distance of 2.09 Å, and Si atoms in the second coordination shell at 3.2 Å, which can be expected for Ni^{2+} cations attached to the zeolite framework via Ni–O–Si bridges. The FEFF model included two single scattering paths and all significant multiple scattering paths within the octahedra of the nearest oxygen neighbors up to 3.6 Å, with 8 variable parameters: coordination shell distances (R), coordination numbers (N) and Debye–Waller factors (σ^2) of the two single scattering paths, and the shift of the energy origin of the photoelectron ΔE_o, common to all scattering paths. The amplitude reduction factor S_0^2 was kept fixed at the value 0.90 obtained for the crystalline NiO sample. The parameters of multiple scattering paths within the octahedra of the nearest oxygen neighbours were constrained with the values of structural parameters obtained by modelling the single scattering paths on the same neighbours.

The FEFF model describes very well the EXAFS spectrum of the Ni/05ZSM-5-1 sample in the k range of 3–14 Å^{-1} and the R-range of 1.2–3.2 Å (Fig. 6 and S3†). The best fit structural parameters are given in Table S3.† The results show that Ni cations are octahedrally coordinated with 6 oxygen atoms at 2.05 Å, and two Si neighbours are detected at 3.17 Å. The signal of the Si neighbours is relatively weak due to a large Debye–Waller factor (0.017), indicating large disorder in the Si coordination shell. In the fitting, we also tested for the presence of Ni neighbours in the second coordination shell, but the contribution of the Ni backscattering was ruled out because of the poor fit results. So, we can conclude that in the Ni/05ZSM-5-1 sample, all Ni cations are attached to the zeolite framework via Ni–O–Si bridges. The absence of Ni–O–Ni coordination shows that the sample contains no NiO nanoparticles. The results are supported also by the STEM and EDX images of the Ni/05ZSM-5-1 sample (Fig. 3i–p), which show that the sample Ni/05ZSM-5-1 contains no NiO nanoparticles and that Ni is distributed uniformly.

The EXAFS spectra of all other Ni/ZSM-5 samples were modelled with the combined FEFF model that contained all scattering paths used in the fit of the crystalline NiO (in which the coordination numbers of each shell were also allowed to vary) and scattering paths of O and Si neighbours found in the case of the Ni/05ZSM-5-1 sample where Ni^{2+} cations are attached to the zeolite framework via Ni–O–Si bridges. Very good EXAFS fits (Fig. 6) are obtained in the k range of 3–14 Å^{-1} and the R-range of 1.2–3.3 Å. The best fit structural parameters are listed in Table S4.† The results of EXAFS analyses show that in all samples, Ni cations are coordinated with six oxygen atoms in the first coordination shell and Ni and O neighbours in more distant coordination shells, at distances characteristic of the Ni

oxide crystal structure. However, the coordination numbers of Ni and oxygen shells at larger distances are significantly lower than that in the bulk NiO. (The EXAFS model, where coordination numbers of Ni and O neighbours in the second and third coordination shells are constrained to the NiO crystallographic values, is excluded by the fit, since it cannot describe the reduced signal of these coordination shells.) No Si neighbours in the second coordination shell could be unambiguously detected. Most probably, their signal is below the detection limit due to the large Debye–Waller factor, as observed in the case of the Ni/05ZSM-5-1 sample. So, we have to point out that the presence of Ni cations directly attached to the zeolite framework by Ni–O–Si bridges is not excluded by the EXAFS fit.

According to XAS analysis, the lower average coordination numbers of more distant Ni and O coordination shells compared to that in the bulk NiO can be explained by two possible structural situations: the first possibility is that all Ni cations are incorporated in small crystalline NiO nanoparticles with different sizes below 2 nm,[45–47] whereas the second possibility is that the samples contain a mixture of larger NiO crystalline nanoparticles and Ni cations directly attached to the zeolite framework, as in the case of the Ni/05ZSM-5-1 sample. However, because STEM and XRD analyses show that NiO nanoparticles present in the samples have significantly larger sizes than 2 nm, in fact they range between 3 and 50 nm, we can conclude that the catalyst samples contain a mixture of the two phases (large NiO nanoparticles and Ni cations directly attached to the ZSM-5 zeolite framework *via* Ni–O–Si bridges) with different relative ratios between them. In this case, the ratio of the two Ni-containing phases can be estimated from average coordination numbers of Ni neighbours in the second coordination shell (Table S4†). The results are presented in Table 5.

The average coordination number of the nearest oxygen coordination shell is 6 in all samples, which is expected for the mixture of the two phases, since Ni is octahedrally coordinated with six oxygen atoms in both phases. In the samples with significantly lower Ni and O coordination numbers in more distant coordination shells (*i.e.*, lower relative amount of NiO

crystalline nanoparticles), we detected a slightly shorter average Ni–O distance in the first coordination shell compared to that in the NiO bulk crystal (2.080 Å), closer to the value of the Ni–O distance found in the Ni/05ZSM-5-1 sample (2.053 Å), where all Ni cations form Ni–O–Si bridges to the zeolite framework.

The EXAFS results and conclusion are supported by Ni K-edge XANES analysis, which showed that a linear combination of the XANES profiles of the reference NiO nanoparticles and Ni/05ZSM-5-1 sample can describe the XANES spectra of all the samples. Considering that the reference XANES spectrum of NiO nanoparticles on the CeO_2 support is a good approximation for the large NiO crystalline nanoparticles in the samples, and the spectrum of the Ni/05ZSM-5-1 sample represents the reference for Ni cations attached to the zeolite framework *via* Ni–O–Si bridges, without any NiO nanoparticles, as indicated by EXAFS analysis, then we can conclude that the results of LCF analysis of the XANES spectra of Ni/ZSM-5 samples (Table 4) represent the relative amount of NiO nanoparticles and Ni cations directly attached to the zeolite in the samples. The estimated relative amount of the NiO nanocrystalline phase estimated by XANES analysis matches very well the corresponding values obtained by EXAFS analysis in all samples. The relative ratios between both Ni phases estimated by XANES and EXAFS analysis reveal the same trend in the Ni/ZSM-5 sample series.

The relative ratio between the two Ni phases changes with the Al to Si molar ratios. At a low Al to Si molar ratio, n_{Al}/n_{Si} ≤0.05 (Ni/03ZSM and Ni/04ZSM samples), the NiO nanoparticles predominate in the samples and account for over 65% of Ni phases. Additionally, the fraction of NiO and Ni^{2+} cations attached to the ZSM-5 framework is similar for all the samples irrespective of n_{Al}/n_{Si} and Ni content. However, a considerable difference is observed for the 05ZSM-5 series possessing the highest n_{Al}/n_{Si} (0.08) molar ratio. In contrast with the 03ZSM-5 and 04ZSM-5 series, the majority of Ni introduced in 05ZSM is attached to the ZSM-5 framework, ranging from about 59% to 100%. This is probably associated with the higher number of framework negative charges available due to a higher number of Al in the framework as mentioned above. Moreover, with gradually increasing Ni content in the 05ZSM-5 series, the fraction of NiO increases from 0 to about 41%, which indicates that Ni fills in the charge compensating positions first and then forms NiO nanoparticles at an excess amount of Ni. The obtained results suggest a strong influence of Al content on the amount of NiO in the form of nanoparticles, which is reported to be more reducible and active than Ni^{2+} attached to the ZSM-5 zeolite framework.[19,25] The NiO content should, therefore, be used as a measure of the hydrogenation activity instead of the bulk Ni content as often reported. A follow up study to confirm our hypothesis on the influence of Al on Ni phases and thus the resulting catalytic activity is in preparation.

Conclusions

In summary, the combination of the characterization techniques, XAS, XRD and TEM, sheds additional light on understanding the alteration of Ni-containing phases upon varying the Al to Si molar ratio (n_{Al}/n_{Si} ≤0.08) in ZSM-5 zeolites. The

Table 5 Relative amount of NiO crystalline nanoparticles and Ni^{2+} attached to the ZSM-5 zeolite framework estimated from average coordination numbers of Ni neighbours in the second coordination shell, determined by EXAFS analysis (Table S3). Uncertainty of relative amounts is ±5%

	Relative amount/%	
Samples	NiO	Ni^{2+} attached to the ZSM-5 zeolite framework
Ni/03ZSM-5-1	71%	29%
Ni/03ZSM-5-3	75%	25%
Ni/03ZSM-5-5	71%	29%
Ni/04ZSM-5-1	73%	27%
Ni/04ZSM-5-3	75%	25%
Ni/04ZSM-5-5	72%	28%
Ni/05ZSM-5-1	0%	100%
Ni/05ZSM-5-3	35%	65%
Ni/05ZSM-5-5	41%	59%

structural and textural properties of ZSM-5 are preserved to a large extent after Ni introduction *via* incipient wetness impregnation. The impregnated Ni species are present in two phases: (1) cubic NiO nanocrystals (size of 3–50 nm) with a *Fm3m* space group and a lattice constant $a = 4.177$ Å, and (2) Ni^{2+} cations attached to the zeolite framework as charge compensating cations forming Ni–O–Si bridges. The Ni–O–Si bridges were directly detected by Ni K-edge EXAFS analysis only in the sample Ni/05ZSM-5-1, where no NiO nanocrystals were formed (at least within the detection limit of EXAFS). In the other samples, the relative amount of the two Ni phases is determined by a combined Ni K-edge XANES and EXAFS analysis, complemented by the TEM and XRD results. The difference in the relative amount of the two Ni-containing phases is marginal when increasing Ni content (<3.7 wt%) impregnated in Si-rich ZSM-5 zeolites ($n_{Al}/n_{Si} = 0.03$ and 0.05). In contrast, at a high Al to Si molar ratio (0.08), a clear trend was observed with increasing Ni content in 05ZSM-5. Ni^{2+} cations were first incorporated as charge compensating cations onto the ZSM-5 framework, and then the excess amount of Ni was deposited in the form of NiO nanocrystals. At a given nominal Ni content, a higher Al to Si molar ratio results in a lower relative amount of NiO in Ni/ZSM-5 due to the higher share of Ni^{2+} as charge compensating cations. The number of NiO nanocrystals, which is highly reducible in comparison to charge compensating Ni^{2+} cations, is proven to highly depend on the Al to Si molar ratio (Al content). Thus, care must be taken to interpret any changes in catalytic activity upon varying Al content or Al to Si ratios of ZSM-5, as it affects both the acid and redox functionalities of the bifunctional Ni/ZSM-5 catalysts. The interdependence of Ni phases and Al content might also apply to other types of metals and/or zeolites, which requires further investigation.

Experimental section

Synthesis of ZSM-5 zeolites

ZSM-5-type zeolites were prepared following a procedure previously reported by Fakin *et al.*[39] The molar ratio of the synthesis gels or "synthesis recipe" is 11.5 Na_2O: xAl_2O_3: 100 SiO_2: $4000H_2O$. x was varied from 1.5 to 2 and 2.5 in order to obtain ZSM-5 zeolites with different Al to Si molar ratios, *i.e.*, $n_{Al}/n_{Si} = 0.03$, 0.04 and 0.05, respectively. The obtained materials were referred to as 03ZSM-5, 04ZSM-5 and 05ZSM-5, respectively. Typically, a sufficient amount of ZSM-5 crystallization seeds (ZAD-MFI-30), *i.e.*, 0.35 wt% of the total mass of the synthesis gels, is dispersed in deionized water at room temperature (RT) for 5 minutes. Subsequently, sodium aqueous glass (NaVS-3M (Silkem), $\omega_{Na_2O} = 8.33$ wt%, and $\omega_{SiO_2} = 27.18$ wt%) is added under continuous stirring conditions for 5 minutes. To the resultant mixture, an aqueous solution of sodium aluminate (Silkem, $\rho = 1335$ g L^{-1}, $\gamma_{Na_2O} = 175.93$ g L^{-1} and $\gamma_{Al_2O_3} = 151.57$ g L^{-1}) is added and stirred for 10 minutes. Sulfuric acid (Sigma Aldrich, 96%) is slowly added to the mixture until the gel is formed. The amount of sulfuric acid is equivalent to the excess amount of Na_2O in the mixture with respect to that of the "synthesis recipe". The gel is aged for 30 minutes at RT. After aging, the gel is transferred into a Teflon

liner, which is subsequently placed into an autoclave. The crystallization is carried out at 180 °C for 24 h. The resultant mixture is later filtered, washed with deionized water and dried at 90 °C for 12 h. The obtained solids are in the Na^+ form.

H^+ form zeolites (H-ZSM-5) were prepared by NH_4^+ ion exchange followed by thermal treatment. A mixture of the Na^+ form zeolite, ammonium sulphate ((NH_4)$_2SO_4$, Sigma Aldrich, ≥99.0%) and deionized water with a mass ratio of 1 : 1 : 20, respectively, was stirred at 30 °C for 2 h. Subsequently, the mixture was filtered, washed with deionized water and dried overnight at 105 °C. The solid was then calcined at 550 °C (heating ramp of 5 °C min^{-1}) for 2 h in air.

Introduction of Ni *via* incipient wetness impregnation

The materials consisting of Ni supported on ZSM-5 were synthesized by incipient wetness impregnation. First, H-ZSM-5 zeolites were preheated in an oven at 60 °C for 15 minutes. A predetermined amount of the Ni precursor (Ni(NO_3)$_2$·$6H_2O$, Sigma Aldrich, 99.999%), was dissolved in 1 mL of deionized water.

The prepared Ni solution was added to H-ZSM-5 dropwise and under vigorous stirring. The mixture was dried overnight at RT. Finally, the solid was calcined in air at 500 °C for 2 h. The amount of the Ni precursor was varied in order to obtain various molar ratios of Ni to Si of 0.01, 0.03 and 0.05. The obtained products were, therefore, labelled as Ni/ZSM-5-1, Ni/ZSM-5-3 and Ni/ZSM-5-5, respectively. Taking 04ZSM-5 as an example, after the impregnation of Ni, Ni/04ZSM-5-1, Ni/04ZSM-5-3 and Ni/04ZSM-5-5 are obtained.

Characterization of Ni supported on ZSM-5 materials

The structural properties of all investigated catalysts were characterized by using a PANalytical X'Pert PRO MPD X-ray diffractometer (CuK$_{\alpha 1}$ = 0.154 nm). The powder X-ray diffraction patterns were recorded at room temperature in the 2θ range from 5° to 70° with a step size of 0.034°.

N_2 sorption isotherms were recorded on a Quantachrome Autosorb iQ3 gas sorption analyzer at 77 K. Prior to the measurements, the samples were evacuated at 523 K under vacuum for 10 h. The specific surface area (A_{BET}) was calculated using the Brunauer–Emmett–Teller (BET) model. Non-local density functional theory (NLDFT) was employed on the adsorption branch of isotherms to evaluate the cumulative pore volume curve of zeolite materials. Based on the obtained curve, the total pore volume (V_p) and the micropore volume (V_{micro}) were determined according to the pore width corresponding to $p/p_0 = 0.95$ and the volume adsorbed at the pore width of 2 nm, respectively. The mesopore volume (V_{meso}) was subsequently calculated by the subtraction of V_{micro} from V_p, *i.e.*, $V_{meso} = V_p - V_{micro}$.

The Ni K-edge XANES (X-ray absorption near edge structure) and EXAFS (extended X-ray absorption fine structure) spectra of different Ni/ZSM-5 zeolite catalysts and the reference NiO crystalline and NiO nanocrystalline (4 wt% NiO on the CeO_2 support) samples were measured at the XAFS beamline of the Elettra synchrotron in Trieste in the transmission detection mode at

room temperature. The samples were prepared in the form of homogeneous pellets with an optimal total absorption thickness of about 2 above the investigated absorption edge. The Ni K-edge jump in the spectra varied in the range between 0.1 and 0.5, depending on the concentration of Ni in the samples.

A Si (111) double crystal monochromator was used with about 1 eV resolution at the Ni K-edge (8333 eV). The intensity of the monochromatic X-ray beam was measured by using three 30 cm long ionization detectors, filled with the following gas mixtures: (first) 580 mbar N_2 and 1420 mbar He; (second) 90 mbar Ar, 910 mbar He, and 1000 mbar N_2; (third) 350 mbar Ar, 1000 mbar N_2, and 650 mbar He. The sample pellets were placed in the beam between the first two ionization detectors. The absorption spectra were measured in the energy region from −150 eV to +1000 eV relative to the investigated absorption edge. In the XANES region, equidistant energy steps of 0.2 eV were used, while for the EXAFS region, equidistant k steps of 0.03 Å^{-1} were adopted, with an integration time of 1 s per step. Three to six repetitions of each scan were recorded to improve the signal to noise ratio. The exact energy calibration was established with simultaneous absorption measurement on Ni metal foil placed between the second and the third ionization chamber. Absolute energy reproducibility of the measured spectra was ±0.005 eV. The analysis of the XANES and EXAFS spectra was performed with the Demeter (IFFEFIT) program package[48] in combination with the FEFF6 program code[44] for *ab initio* calculation of photoelectron scattering paths.

A Varian 600 MHz NMR spectrometer (Varian, USA) was employed to collect ^{27}Al magic angle spinning – nuclear magnetic resonance spectra (MAS-NMR). The ^{27}Al Larmor frequency was 156.17 MHz. The spectra were recorded at a sample rotation frequency of 20 kHz, with a recycle time of 5 s and a total number of scans of 480. The obtained spectra were referenced to the signal of Al nuclei of 1 M solution of Al(NO$_3$)$_3$ in water.

Scanning transmission electron microscopy (STEM) analysis was performed with a Cs probe-corrected TEM/STEM Jeol ARM 200 CF microscope with a cold-FEG electron source, operated at 80 kV. A Jeol Centurio 100 mm^2 Energy dispersive X-ray spectrometer (EDXS) was used for elemental analyses and mapping in the scanning-transmission mode (STEM). The samples in the powder form were dispersed in ethanol and placed on a copper lacy-carbon coated TEM grid.

Energy dispersive X-ray (EDX) spectroscopy was performed on a Zeiss Supra 35 VP microscope (acceleration voltage 20 kV) equipped with a 100 mm^2 silicon drifted detector (SDD). The samples were compressed into pellets with a diameter of 6 mm and a thickness of 1 to 2 mm. Prior to recording the spectra, the pellets were coated with carbon. For each sample, EDX spectra were recorded at 5 different sites of interest and evaluated with the INCA software.

Author contributions

Conceptualization and methodology: N. N. T., H.-T. V. and I. A.; formal analysis: H.-T. V., I. A., G. D, and J. V.; writing – original draft preparation: H.-T. V., I. A. and G. D.; synchrotron XAS measurements: D. O. S and S. P; writing – review and editing: G. M., N. Z. L. and N. N. T.; visualization: H.-T. V.; project administration: N. N. T.; funding acquisition: N. Z. L.; All authors have read and agreed to the published version of the manuscript.

Conflicts of interest

There are no conflicts to declare.

Acknowledgements

References

1 A. Lambin and J.-M. Corpart, UN sustainable development goals and green chemistry, key points for sustainably innovating at Roquette, a global leader in plant-based ingredients, *Current Opinion in Green and Sustainable Chemistry*, 2018, **13**, 137–139.

2 J. H. Clark, T. J. Farmer, L. Herrero-Davila and J. Sherwood, Circular economy design considerations for research and process development in the chemical sciences, *Green Chem.*, 2016, **18**, 3914–3934.

3 J. García–Martínez, Chemistry 2030: A Roadmap for a New Decade, *Angew. Chem.*, 2021, **133**, 5008–5012.

4 K. Kümmerer, J. H. Clark and V. G. Zuin, Rethinking chemistry for a circular economy, *Science*, 2020, **367**, 369–370.

5 G. Salviulo, M. C. Lavagnolo, M. Dabalà, E. Bernardo, A. Polimeno, M. Sambi, F. Bonollo and S. Gross, Enabling Circular Economy: The Overlooked Role of Inorganic Materials Chemistry, *Chem. –Eur. J.*, 2021, **27**, 6676–6695.

6 T. Ennaert, J. van Aelst, J. Dijkmans, R. de Clercq, W. Schutyser, M. Dusselier, D. Verboekend and B. F. Sels, Potential and challenges of zeolite chemistry in the catalytic conversion of biomass, *Chem. Soc. Rev.*, 2016, **45**, 584–611.

7 G. Ertl, H. Knzinger, F. Schüth and J. Weitkamp, *Handbook of Heterogeneous Catalysis*, Wiley-VCH Verlag GmbH & Co. KGaA, Weinheim, Germany, 2008.

8 J. Čejka, R. E. Morris and P. Nachtigall, *Zeolites in catalysis. Properties and applications*, Royal Society of Chemistry, Cambridge, 1st edn, 2017.

9 J. Weitkamp and L. Puppe, *Catalysis and Zeolites*, Springer, New York, 1999.

10 A. W. Chester and E. G. Derouane, *Zeolite Chemistry and Catalysis*, Springer Netherlands, Dordrecht, 2009.

11 B. Sels and M. van de Voorde, *Nanotechnology in Catalysis: Application in the Chemical Industry, Energy Development, and Environment Protection*, Wiley-VCH Verlag GmbH & Co. KGaA, Weinheim, Germany, 2017.

12 C. G. Lima, N. M. Moreira, M. W. Paixão and A. G. Corrêa, Heterogenous green catalysis: Application of zeolites on multicomponent reactions, *Current Opinion in Green and Sustainable Chemistry*, 2019, **15**, 7–12.

13 D. Liu, L. Cao, G. Zhang, L. Zhao, J. Gao and C. Xu, Catalytic conversion of light alkanes to aromatics by metal-containing HZSM-5 zeolite catalysts—A review, *Fuel Process. Technol.*, 2021, **216**, 106770.

14 X. Li, G. Chen, C. Liu, W. Ma, B. Yan and J. Zhang, Hydrodeoxygenation of lignin-derived bio-oil using molecular sieves supported metal catalysts: A critical review, *Renewable Sustainable Energy Rev.*, 2017, **71**, 296–308.

15 W. Luo, W. Cao, P. C. A. Bruijnincx, L. Lin, A. Wang and T. Zhang, Zeolite-supported metal catalysts for selective hydrodeoxygenation of biomass-derived platform molecules, *Green Chem.*, 2019, **21**, 3744–3768.

16 D. Kiani, S. Sourav, Y. Tang, J. Baltrusaitis and I. E. Wachs, Methane activation by ZSM-5-supported transition metal centers, *Chem. Soc. Rev.*, 2021, **50**, 1251–1268.

17 S. Dutta, I. K. Yu, D. C. Tsang, Y. H. Ng, Y. S. Ok, J. Sherwood and J. H. Clark, Green synthesis of gamma-valerolactone (GVL) through hydrogenation of biomass-derived levulinic acid using non-noble metal catalysts: A critical review, *Chem. Eng. J.*, 2019, **372**, 992–1006.

18 A. J. Maia, B. G. Oliveira, P. M. Esteves, B. Louis, Y. L. Lam and M. M. Pereira, Isobutane and n-butane cracking on Ni-ZSM-5 catalyst: Effect on light olefin formation, *Appl. Catal., A*, 2011, **403**, 58–64.

19 A. J. Maia, B. Louis, Y. L. Lam and M. M. Pereira, Ni-ZSM-5 catalysts: Detailed characterization of metal sites for proper catalyst design, *J. Catal.*, 2010, **269**, 103–109.

20 A. J. Maia, E. B. Pereira, A. C. Sola, N. Homs, P. R. de La Piscina, B. Louis and M. M. Pereira, Understanding bifunctional behavior of Ni/HZSM5 catalyst under isobutane atmosphere, *Mol. Catal.*, 2018, **458**, 145–151.

21 G. Vitale, H. Molero, E. Hernandez, S. Aquino, V. Birss and P. Pereira-Almao, One-pot preparation and characterization of bifunctional Ni-containing ZSM-5 catalysts, *Appl. Catal., A*, 2013, **452**, 75–87.

22 A. Masalska, Ni-loaded catalyst containing ZSM-5 zeolite for toluene hydrogenation, *Appl. Catal., A*, 2005, **294**, 260–272.

23 M. M. Yung, A. K. Starace, C. Mukarakate, A. M. Crow, M. A. Leshnov and K. A. Magrini, Biomass Catalytic Pyrolysis on Ni/ZSM-5: Effects of Nickel Pretreatment and Loading, *Energy Fuels*, 2016, **30**, 5259–5268.

24 S. Fadaeerayeni, J. Shan, E. Sarnello, H. Xu, H. Wang, J. Cheng, T. Li, H. Toghiani and Y. Xiang, Nickel/gallium modified HZSM-5 for ethane aromatization: Influence of metal function on reactivity and stability, *Appl. Catal., A*, 2020, **601**, 117629.

25 A. Jentys, A. Lugstein and H. V. Vinek, Characterization of metallic species on Ni- and Co-containing ZSM-5 catalysts—reduction behavior and catalytic properties, *Zeolites*, 1997, **18**, 391–397.

26 S.-K. Ihm, K.-H. Yi and Y.-K. Park, in *Zeolites and Related Microporous Materials: State of the Art 1994 - Proceedings of the 10th International Zeolite Conference, Garmisch-Partenkirchen, Germany*, Elsevier, 17-22 July 1994, pp. 1765–1772.

27 M. Li, S. Xing, L. Yang, J. Fu, P. Lv, Z. Wang and Z. Yuan, Nickel-loaded ZSM-5 catalysed hydrogenation of oleic acid: The game between acid sites and metal centres, *Appl. Catal., A*, 2019, **587**, 117112.

28 A. Kostyniuk, D. Bajec and B. Likozar, Catalytic hydrogenation, hydrocracking and isomerization reactions of biomass tar model compound mixture over Ni-modified zeolite catalysts in packed bed reactor, *Renewable Energy*, 2021, **167**, 409–424.

29 Z.-P. Hu, C.-C. Weng, C. Chen and Z.-Y. Yuan, Catalytic decomposition of ammonia to COx-free hydrogen over Ni/ZSM-5 catalysts: A comparative study of the preparation methods, *Appl. Catal., A*, 2018, **562**, 49–57.

30 V. K. Velisoju, D. Jampaiah, N. Gutta, U. Bentrup, A. Brückner, S. K. Bhargava and V. Akula, Conversion of γ-Valerolactone to Ethyl Valerate over Metal Promoted Ni/ZSM-5 Catalysts: Influence of Ni0/Ni2+ Heterojunctions on Activity and Product Selectivity, *ChemCatChem*, 2020, **12**, 1341–1349.

31 Q. Wei, P. Zhang, X. Liu, W. Huang, X. Fan, Y. Yan, R. Zhang, L. Wang and Y. Zhou, Synthesis of Ni-Modified ZSM-5 Zeolites and Their Catalytic Performance in n-Octane Hydroconversion, *Front. Chem.*, 2020, **8**, 586445.

32 A. Masalska, K. Jaroszewska and J. R. Grzechowiak, Physicochemical and Catalytic Properties of Ni,H/ZSM-5 and Ni,H/ZSM-5–Binder Catalysts Prepared in the Absence and in the Presence of Binder, *Kinet. Catal.*, 2019, **60**, 851–861.

33 J. F. Da Costa-Serra, C. Cerdá-Moreno and A. Chica, Zeolite-Supported Ni Catalysts for CO2 Methanation: Effect of Zeolite Structure and Si/Al Ratio, *Appl. Sci.*, 2020, **10**, 5131.

34 Y. Shi, C. Gao, E. Xing, J. Zhang, F. Duan, H. Zhao and Y. Xie, Ni nanoparticles encapsulated within H-type ZSM-5 crystals for upgrading palmitic acid to diesel-like fuels, *Chin. Chem. Lett.*, 2022, **33**, 803–806.

35 W. Li, H. Wang, X. Wu, L. E. Betancourt, C. Tu, M. Liao, X. Cui, F. Li, J. Zheng and R. Li, Ni/hierarchical ZSM-5 zeolites as promising systems for phenolic bio-oil upgrading: Guaiacol hydrodeoxygenation, *Fuel*, 2020, **274**, 117859.

36 X. Zhu, Y. Wang, G. Wang, Y. Hou, M. Yu, X. Yang and F. Yin, Synergistic co-conversion of pentane and methanol to

aromatics over bifunctional metal/ZSM-5 zeolite catalysts, *Microporous Mesoporous Mater.*, 2021, **320**, 111107.

37 D. E. Perea, I. Arslan, J. Liu, Z. Ristanović, L. Kovarik, B. W. Arey, J. A. Lercher, S. R. Bare and B. M. Weckhuysen, Determining the location and nearest neighbours of aluminium in zeolites with atom probe tomography, *Nat. Commun.*, 2015, **6**, 7589.

38 L. Shirazi, E. Jamshidi and M. R. Ghasemi, The effect of Si/Al ratio of ZSM-5 zeolite on its morphology, acidity and crystal size, *Cryst. Res. Technol.*, 2008, **43**, 1300–1306.

39 T. Fakin, A. Ristić, V. Mavrodinova and N. Zabukovec Logar, Highly crystalline binder-free ZSM-5 granules preparation, *Microporous Mesoporous Mater.*, 2015, **213**, 108–117.

40 P. A. Jacobs and J. A. Martens, in *Studies in Surface Science and Catalysis: Synthesis of High-Silica Aluminosilicate Zeolites*, ed. P. A. Jacobs and J. A. Martens, Elsevier, 1987, pp. 47–111.

41 H.-T. Vu, F. M. Harth, M. Goepel, N. Linares, J. García-Martínez and R. Gläser, Enhanced activity of a bifunctional Pt/zeolite Y catalyst with an intracrystalline hierarchical pore system in the aqueous-phase hydrogenation of levulinic acid, *Chem. Eng. J.*, 2022, **430**, 132763.

42 T. Kyômen, R. Yamazaki and M. Itoh, Valence and spin state of Co and Ni ions and their relation to metallicity and ferromagnetism in LaCo0.5Ni0.5O3, *Phys. Rev. B*, 2003, **68**, 104416.

43 S. Sasaki, K. Fujino and Y. Takéuchi, X-ray determination of electron-density distributions in oxides, MgO, MnO, CoO, and NiO, and atomic scattering factors of their constituent atoms, *Proc. Jpn. Acad., Ser. B*, 1979, **55**, 43–48.

44 J. J. Rehr, R. C. Albers and S. I. Zabinsky, High-order multiple-scattering calculations of x-ray-absorption fine structure, *Phys. Rev. Lett.*, 1992, **69**, 3397–3400.

45 A. Kuzmin and J. Chaboy, EXAFS and XANES analysis of oxides at the nanoscale, *IUCrJ*, 2014, **1**, 571–589.

46 Y. Lyu, J. Jocz, R. Xu, E. Stavitski and C. Sievers, Nickel Speciation and Methane Dry Reforming Performance of Ni/Ce$_x$ Zr$_{1-x}$O$_2$ Prepared by Different Synthesis Methods, *ACS Catal.*, 2020, **10**, 11235–11252.

47 A. Barbier, A. Tuel, I. Arcon, A. Kodre and G. A. Martin, Characterization and Catalytic Behavior of Co/SiO2 Catalysts: Influence of Dispersion in the Fischer–Tropsch Reaction, *J. Catal.*, 2001, **200**, 106–116.

48 B. Ravel and M. Newville, ATHENA, ARTEMIS, HEPHAESTUS: data analysis for X-ray absorption spectroscopy using IFEFFIT, *J. Synchrotron Radiat.*, 2005, **12**, 537–541.